Extreme Mechanics Letters 71 (2024) 102208

Contents lists available at ScienceDirect

Extreme Mechanics Letters

journal homepage: www.elsevier.com/locate/eml

Fully dense and cohesive FCC granular crystals

Ashta Navdeep Karuriya, Jeremy Simoes, Francois Barthelat *

Department of Mechanical Engineering, University of Colorado, 427 UCB, 1111 Engineering Dr, Boulder, CO 80309, United States

ARTICLE INFO

Keywords:
Cohesive granular crystals
Granular materials
Crystal plasticity
Granular metamaterials
Architectured materials

ABSTRACT

Typical granular materials are far from optimal in terms of mechanical performance: Random packing leads to poor load transfer in the form of thin and dispersed force lines within the material, to inhomogeneous jamming, and to strain localization. In addition, localized contacts between individual grains result in low stiffness, strength and brittleness. Here we propose a granular material that simultaneously embodies three approaches to increase strength: geometrical design of individual grains, crystallization, and infiltration by an adhesive. Using mechanical vibrations, we assembled millimeter-scale 3D printed grains with rhombic dodecahedral shapes into fully dense FCC granular crystals. We then infiltrated the granular structure with a tacky, polyacrylic adhesive that is orders of magnitude weaker than the grains, but which provides sustained adhesion over large interfacial displacements. The resulting material is a fully dense, free-standing space filling granular crystal. Compressive tests show that these granular crystals are up to 60 times stronger than randomly packed cohesive spheres and they display a rich set of mechanisms: Nonlinear deformations, crystal plasticity reminiscent of atomistic mechanisms, cross-slip, shear-induced dilatancy, micro-buckling, and tensile strength. To capture some of these mechanisms we developed a multiscale model that incorporates local cohesion between grains, resolved shear and normal stresses on available slip planes, and prediction of compressive strength as function of loading orientation. The predicted strength is highly anisotropic and agrees well with the compression experiments. Once fully understood and harnessed, we envision that these mechanisms will lead to granular engineering materials with unusual combinations of mechanical performances attractive for many applications.

1. Introduction

Granular materials can be defined as a large collection of discrete, macroscopic particles which are in general non-cohesive. These materials, ubiquitous in everyday life and in industry (food, pharmaceutics, powder metallurgy, geology, mining…), are seemingly simple, but they in fact display a wide range of complex mechanical responses. For example, granular materials can be as stiff as a solid, or they can flow like a liquid depending on confinement [1]. Granular materials also display interesting deformation mechanisms: shear bands, jamming, localized regions of stress transfer, clusters formations, shear induced dilatation [2,3]. The poor packing of typical granular materials, however, limits their strength and mechanical performance. In typical granular solids applied stresses are transferred along thin "force chain lines" [4], while most of grains remain free of stress. One approach to increase strength is to promote jamming by designing the shape of individual grains. For example, convex platonic shapes (cubes, tetrahedra and octahedra) increase the shear strength by 40–80 % in comparison to materials based on spheres [5]. Another approach to increase strength is to infuse the granular assembly with a liquid phase, which enables free-standing structures and further improves mechanical performance and functionalities. For example, internal cohesion from surface tension in wet sand produces tensile strength [6], and fluids with various rheologies including lubrication, viscous flow, or rate dependent behaviors can be exploited to manipulate overall mechanical responses [7–9]. Granular assemblies can also be infiltrated with adhesives (for example, polyborosiloxane (PBS) on spherical glass particles [10,11]), and the mechanical properties of these cohesive granular materials can be tuned via polymer chemistry [12–14]. A third approach to increase the strength of granular materials is to arrange the grains into crystals, which can be induced by mechanical vibrations, gravitational sedimentation or other compaction protocols [15–18]. For example, one-dimensional granular chains [19–21] and granular crystals [22–26] display unusual and useful characteristics in terms of energy absorption, elastic wave propagation, acoustics, or shock waves attenuation. Taking this approach to the extreme, the shape of the individual grains can be

* Corresponding author.
E-mail address: francois.barthelat@colorado.edu (F. Barthelat).

https://doi.org/10.1016/j.eml.2024.102208
Received 25 April 2024; Received in revised form 11 July 2024; Accepted 12 July 2024
Available online 14 July 2024

designed to create near fully dense 2D granular crystals ("Topologically interlocked materials" [27–29]) with enhanced impact resistance [30] or dense and strong 3D granular crystals [31]. In this report, we combine these three approaches (grain shape, crystallization and second adhesive phase) to create strong and free-standing cohesive granular crystals. We first discuss the fabrication of these materials, and we then present grain-on-substrate experiments to characterize the mechanical properties of the pressure sensitive adhesive we selected. We then present and discuss compression tests on the crystals and their non-linear mechanisms, which we captured with a cohesive granular plasticity model.

2. Fabrication of cohesive granular crystals

Fabrication of the granular crystals involved 3D printing, vibration-assisted assembly, and infiltration with a soft adhesive. In this report we focus on fully dense granular crystal with a face-centered cubic (FCC) lattice. The grains were rhombic dodecahedra, a geometry which tessellates space following a FCC spatial arrangement (Fig. 1a). Individual grains were fabricated from an ABS-like photocurable material [32], which is relatively stiff (measured Young's modulus E_g=3 GPa) and strong (measured yield strength = 70 MPa). Individual grains were 3D printed using a digital light processing printer (EnvisionTEC Micro

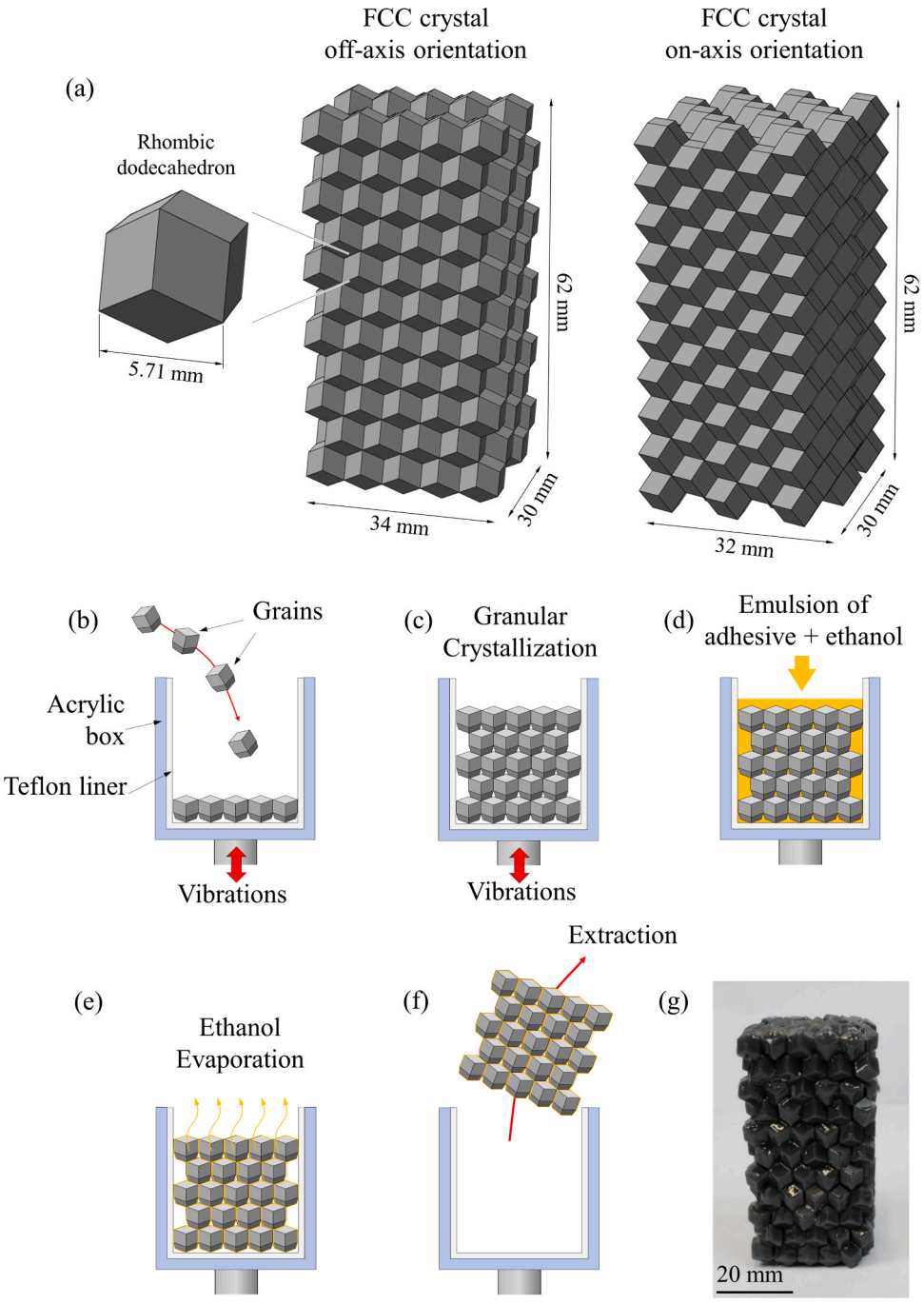

Fig. 1. Overview and fabrication of cohesive granular crystals. (a) Diagram of the individual grain geometry and FCC granular crystals in two different orientations (off-axis and on-axis); Fabrication steps: (b) Grains are poured in the assembly box under vibration; (c) vibration-induced crystallization; (d) An emulsion of adhesive + ethanol is infiltrated into the crystal; (e) The ethanol is evaporated, leaving a thin layer of adhesive at the interfaces; (f) free standing, cohesive granular crystal is extracted from the assembly box; (g) picture of the crystal.

HiRes), which produced fully dense, isotropic grains with smooth surfaces. The grains were then crystallized inside an acrylic assembly box lined with Teflon sheets and attached to a vertical vibration generator. About 30 grains were first dropped into the assembly box, and vibrations with a 2 mm amplitude and at an 18 Hz frequency were generated to start assembly (Fig. 1b). This specific combination of amplitude and frequency was chosen so the grains assembled into a close packed layer at the bottom of the assembly box. Additional grains were then dropped into the box, so the grains assembled, layer-by-layer, into a ~275 grains FCC granular crystal (Fig. 1c).

Once assembly was completed, the vibrations were turned off, and an emulsion of a methacrylate pressure sensitive adhesive (Aleene's Repositionable Tacky Spray [33]) and ethanol solution with a 2:3 ratio by volume was poured onto the crystal. The emulsion had no adhesion and low viscosity, so it fully infiltrated the interfaces of the granular crystal (Fig. 1d). The ethanol was then allowed to fully evaporate for about 72 hours, leaving a thin layer of adhesive at the interfaces of the grains (Fig. 1e). The cohesive granular crystal was then extracted from the assembly box, a process facilitated by the Teflon lining (Fig. 1f). This process produced free standing, single granular FCC crystals (Fig. 1g). The assembly box acted as a strong template for the granular crystallization process. First, the plane of densest packing ({111} plane) always aligned with the horizontal floor of the assembly box. Second, the lines of densest packing within the {111} plane (direction <110>) aligned either with the short vertical wall of the box to produce an "off-axis" crystal, or with the longer vertical wall of the box to produce an "on-axis" crystal (Fig. 1a). We use the "on-axis" terminology because these samples, compressed along the longest dimensions, can be interpreted as a series of stiff columns of grains aligned with the axis of compression. In the "off-axis" direction, these columns of grains are rotated 30° from the axis of loading [31]. We also fabricated cohesive granular samples made of randomly packed spheres (RPS) with the same number of grains as used in cohesive FCC granular crystals. We chose RPS for comparison, since it is a good representation of typical granular materials [2,3], and because previous work on cohesive granular materials were based on RPS [10–13]. For all granular samples we kept the volume of the individual grains constant (V_g= 132 mm^3).

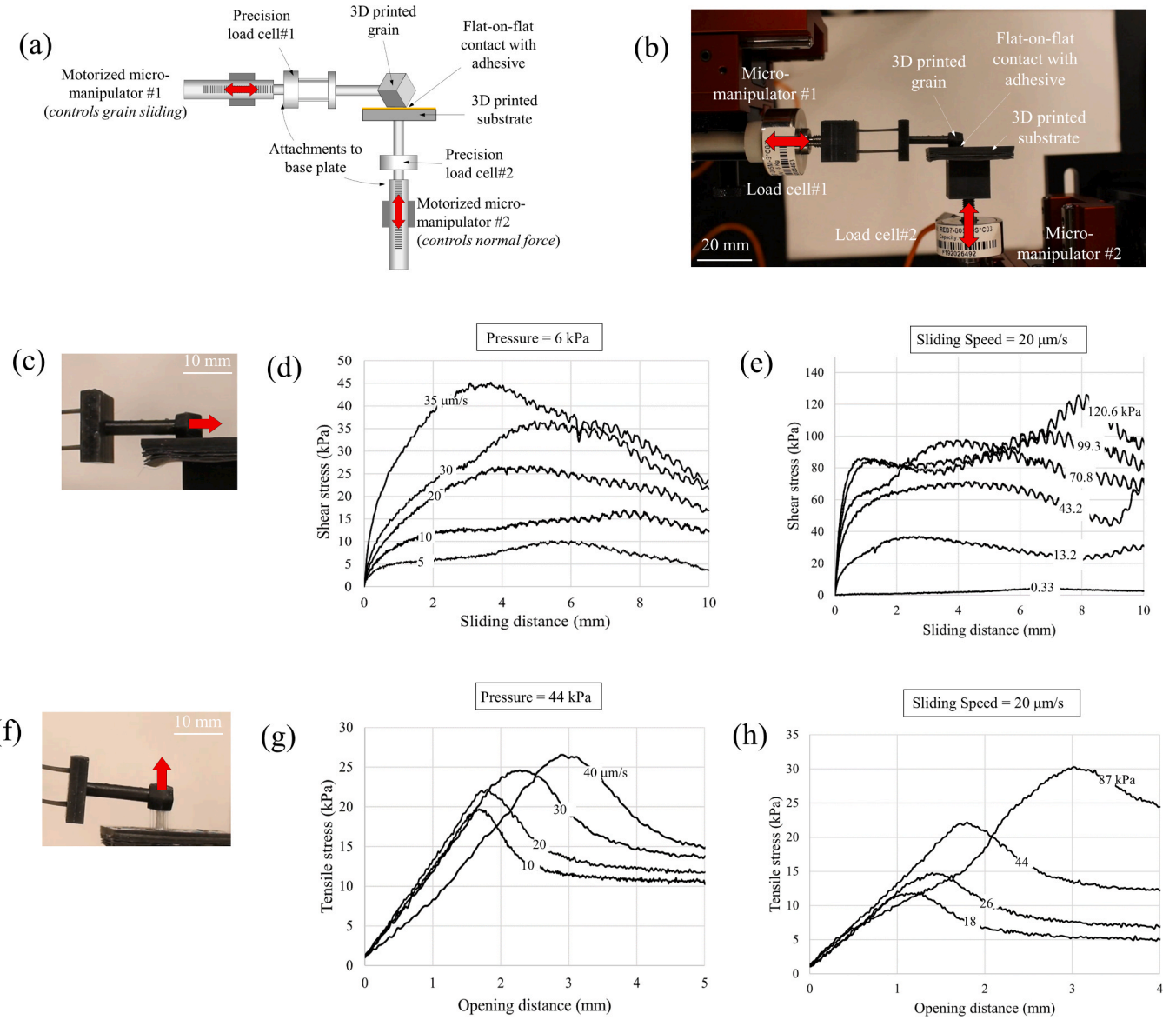

Fig. 2. Grain-on-substrate adhesion tests. (a) Diagram and (b) picture of the experimental setup; (c) shear test configuration and typical responses in shear for (d) different sliding rates and (e) at different applied normal pressures; (f) tensile test configuration and typical tensile responses (g) at different sliding rates and (h) for different normal pressures applied prior to the tensile test.

3. Grain-on-substrate adhesion experiments

The mechanical properties of the cohesive granular crystals are largely governed by the properties of the adhesive used between the grains, which must be carefully selected to achieve controlled, large deformations along interfaces and slip planes within the crystal. To this effect, the adhesive must be weaker than the grains, so that deformation and failure are confined to the interfaces (which, as an added benefit, enables the recycling of the grains). The adhesive must also have a strong adhesion to the grains, and it must sustain cohesive stresses over large sliding distances (several millimeters). Considering that the thickness of the interfaces is in the order of tens of micron, a "ductile" adhesive with extremely high shear strain at failure was required. After consideration of several types of adhesives, we selected a methacrylate-based pressure sensitive adhesive (PSA, Aleene's Repositionable Tacky Spray [33]). PSAs are soft viscoelastic polymers with high molecular weight and low crosslink density [34–37]. PSAs can sustain cohesion over extremely large shear deformations and also large separation distances, by cavitation and by the formation of ligaments [35,36,38,39]. A drawback of this type of adhesives is that they are difficult to characterize and model: their mechanical response is both pressure and rate sensitive. To characterize the mechanical response of the PSA we used in this study, we performed grain-on-substrate mechanical experiments under different loading modes: shear, compression, tension, and under different combinations of shear/compression and shear/tension. Fig. 2a and 2b show an overview of the experimental setup: Grain and substrate were mounted perpendicularly to each other on single axis motorized micro-manipulators, (Sutter Instrument, SOLO-50), so they could be accurately and independently positioned. In addition, a precision load cell was installed in line with each of the micro-manipulators. The adhesive was applied on both the flat substrate, and on one of flat faces of the grain. The substrate was pressed onto the grain using micromanipulator #2 (Fig. 2a) to achieve a flat-on-flat contact and until a desired normal force was reached. The grain was attached using a double beam which could deflect collectively but not rotate, ensuring no rotation of the grain and a uniformly distributed pressure at the grain-substrate interface. Once this initial condition was achieved, the grain was sled onto the substrate using micro-manipulator#1 while the force was recorded. Typical sliding force-displacement curves are shown on Fig. 2d-e. Increasing the sliding distance typically first resulted in an increase of shear stress up to a peak, followed by a gradual decrease in stress. The deformation and failure mechanisms of pressure sensitive adhesive (PSA) are extremely complex and the focus of several recent reports [37,40–42]. These mechanisms involve competitions between rubbery elastic deformations, peeling from the substrate, slippage, and the formation of ligaments. In addition, these mechanisms are highly dependent on crosslinking, deformation rate, confinement and surface roughness of the substrate. In this report we limit the characterization of our PSA to the basic observations and measurements required to understand the mechanics of the granular crystal. The PSA we chose could sustain adhesion over more than 10 mm of sliding distance, again a critical feature to achieve large deformations in the crystals. Plastic deformation of the PSA starts at a yield point before peak stress is reached, and in addition we found that we can use the PSA multiple times for each test with no change in results for fixed sliding rate and fixed applied normal pressure. As expected, the shear strength of the adhesive was sensitive to sliding rate, as shown on Fig. 2d. The shear stress was also a function of the amount of initial normal pressure applied prior to sliding, as shown on Fig. 2e (shear strength increased when more normal pressure was applied). Using the same experimental setup, we performed tensile tests on the adhesive layer. For these tests an initial pressure was first applied, and the substrate was then pulled away from the grain using micro-manipulator#2. Typical normal separation force-displacement curves are shown on Fig. 2g-h. After an initial increase in stress up to a peak stress, the interface softened as PSA ligaments formed across the interface. Adhesive forces could be sustained over openings in excess of 10 mm. The tensile strength of the adhesive depended on the pull rate and on the normal pressure applied onto the interface prior to the pull. Higher pull rates and higher pre-applied normal pressures resulted in higher tensile strengths.

4. Compressive tests on cohesive granular crystals

Once fabricated, the cohesive granular crystals were tested in uniaxial compression along their long axes, using a standard testing frame (ADMET eXpert 5603). We used quasi-static rates of 30 μm/sec and 330 μm /sec, corresponding to compressive strain rates of 4.8×10^{-4} s^{-1} and 5.3×10^{-3} s^{-1} respectively. Pictures of the samples were acquired at regular intervals during the test. True stress and true strain were calculated from the force and displacements using standard procedure, accounting for the large change in specimen length and changes in cross section observed in the experiments. Fig. 3a shows typical stress-strain curves for on-axis and off-axis FCC crystals. The on-axis samples show a relatively stiff response up to a peak, followed by a sharp drop. Along that loading direction, the crystal can be interpreted as a series of columns in parallel, each column consisting of grains in flat-on-flat contact, with contact surface perpendicular to the axis of the column. The on-axis loading orientation produced the highest stiffness and strength. Fig. 3b shows a series of snapshots taken during the test. Near the peak load, the columns of grains buckled collectively, the onset of buckling being followed by a sharp stress decrease. Off-axis samples, on the other hand, also showed a peak stress, followed by a slower decay (Fig. 3a). The cohesive FCC off-axis samples deformed in a way similar to atomic-scale crystal plasticity where grains were sliding along specific planes (Fig. 3b). The grains started to slide on one another at relatively low applied stresses and this onset of "yielding" was followed by strain hardening until a peak compressive stress reached which was followed by softening (Fig. 3a,c). As the grains sled on one another, the loss of contact area between the grains translated in lower overall stresses. Grain sliding occurred along planes of densest packing {111} in the FCC cohesive crystals, in a way consistent with traditional crystal plasticity. We also observed ligaments of the PSA adhesive forming between grains at large deformation. For comparison we also tested cohesive granular matter made of randomly distributed spheres. The random spheres showed a deformation with a relatively steady flow stress and homogenous "flow" of the grains (Fig. 3a), and a much lower strength: The on-axis cohesive FCC samples were 20–60 times stronger than random spheres, and the off-axis cohesive samples were 4–5 times stronger than random spheres (Fig. 3a). There are two main contributing mechanisms to these improvements: (i) the crystalline arrangement generates highly ordered forces lines within the material, so that every grain carries stress (as opposed to randomly packed materials where stresses are transmitted only along thin force lines in the material, while a large fraction of grains do not carry stresses [4]) and (ii) the flat-on-flat contact areas in the crystals are large and in the order of the size of the grains (as opposed to granular materials based on spherical grains where contact area is relatively small, with a contact radius typically only a small fraction of the radius of the grains). Our previous work on granular crystals suggest that both contributions are critical to producing high strength [31], although the exact contribution of each of these mechanisms is not known.

We also tested the cohesive crystal in tension, along the off-axis direction. The crystal was simply glued onto the loading platforms using our PSA adhesive, and a dog-bone geometry was used for the sample to prevent failure at the platforms (Fig. 3c-d). The mechanical response of the cohesive CRD off-axis samples in tension was similar to their response in compression: tensile stresses increase leading to a peak, followed by slow decay governed by ligaments. The tensile strength (~15 kPa) of the crystal was 3–7 times lower than its compressive strength, and in the order of the tensile strength of the adhesive interface (Fig. 2g). Finally, we also examined the effect of loading rate on cohesive CRD off-axis samples. Fig. 3e shows that compressive stress-strain curves

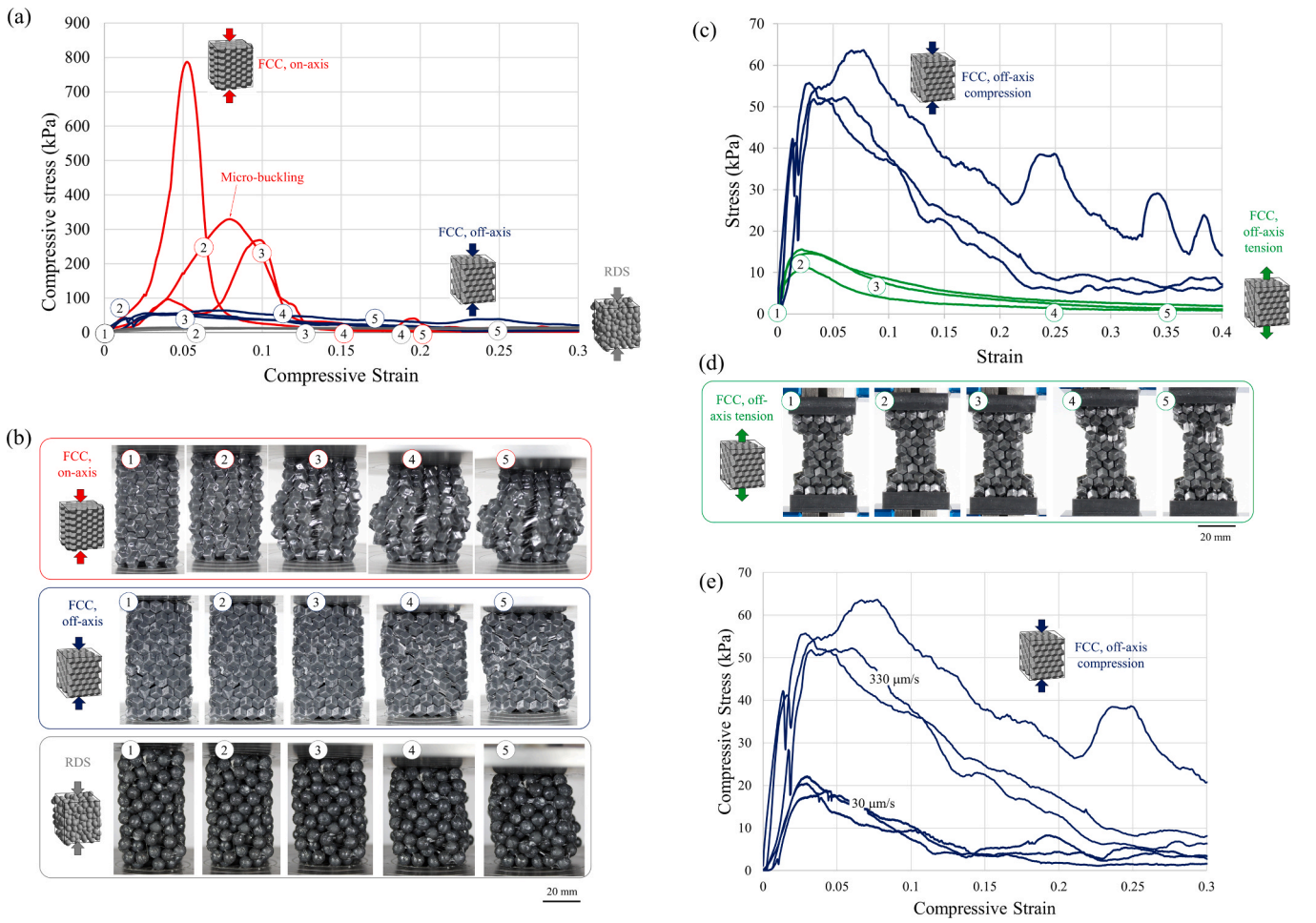

Fig. 3. Compression and tension tests on cohesive granular crystals. (a) Compressive stress-strain curves for cohesive on-axis and off-axis FCC crystals, and randomly distributed spheres (RDS); (b) Snapshots of the samples at different stage of compression reveal a broad range of mechanisms that include micro-buckling, grain-on-grain sliding along slip planes, and dilation; (c) Tensile and compressive stress-strain curves on FCC crystal, off axis; (d) snapshots at different stage of tension; (e) effect of loading rate on compressive response.

are qualitatively similar for two different loading rates, but a 10-fold increase in loading rate resulted in a 2–4-fold increase in compressive strengths. This strong rate dependence was expected because the adhesive is highly sensitive to deformation rate (Fig. 2d). Interestingly, soaking the damaged crystals in ethanol after each test dissolved the adhesive so the grains could be recovered, cleaned and recycled into new cohesive crystals with no loss of mechanical performance.

5. A granular crystal cohesive plasticity model

The mechanics of deformation of the FCC crystal along the off-axis orientation draws similarities with classical crystal plasticity. To further understand and capture this intriguing behavior we developed a "granular crystal cohesive plasticity" model which captured the main mechanism of deformation over the three length scales as shown in Fig. 5a. This model is similar to "granular crystal plasticity" model we developed in our previous work [31]. The main difference in our present model is that, at the smallest scale (level 1), grain-on-grain interactions are governed by adhesion between them (instead of by simple Coulombic frictional contact [31]). At the smallest scale, grain-on-grain interactions govern the response of the granular crystals. The adhesive traction between the grains depends on sliding rate and normal pressure, and also on the sliding distance: As the grain slide on one another their contact area decrease, so that the effective, shear strength should be adjusted by a factor $(1 - u/p)$where u is the sliding distance and p is the length of the partial ($p = 3.5$ mm for the grains tested). Fig. 4b-c show the adjusted shear-sliding curves. We then fitted the shear strength of the grain-on-grain interfaces using a rate and pressure sensitive model (Fig. 4d-e):

$$\tau_i = \tau_0 \left(\frac{\sigma_i}{\sigma_0}\right)^m \left(\frac{\dot{u}_i}{\dot{u}_0}\right)^n \tag{1}$$

Where τ_i is the shear strength of adhesion between two grains, σ_i is the applied normal pressure on a grain and $\dot{u}_i$ is the sliding rate. τ_0, σ_0, $\dot{u}_0$, m and n are adhesive properties identified by curve fitting: $\tau_0 = 0.65$ *kPa*, $\sigma_0 = 1$ *kPa*, $\dot{u}_0 = 1$ μm/sec, $m = 0.6$ and $n = 0.6$.

At level 1, we determined the shear strength of flat-on-flat, grain-on-grain adhesion. At level 2, we considered the non-planar geometry of the {111} slip planes, and possible sliding along one of the three partials in that plane. Fig. 5b shows a {111} plane in gray and an individual grain (in red) belonging to the adjacent {111} plane in the full FCC crystal. A normal stress and a tangential stress are applied onto the red grain which may dislodge it from its original position, and "climb" other grains along a slip direction (more details on this process can be found in [31] for the case of frictional contact). The morphology of the slip plane participates to the resistance to slip, together with the grain-on-grain adhesion model (Eq. (1)), to produce a shear strength $\tau^{(s)}$ as function of the applied normal stress $\sigma^{(s)}$ and the slip velocity or sliding speed $\dot{u}^{(s)}$. These relationships are computed numerically, with the results shown in Fig. 5c. Note that different shearing direction within the {111} plane can produce different resistances to shearing. Lastly, on level 3 of the model a

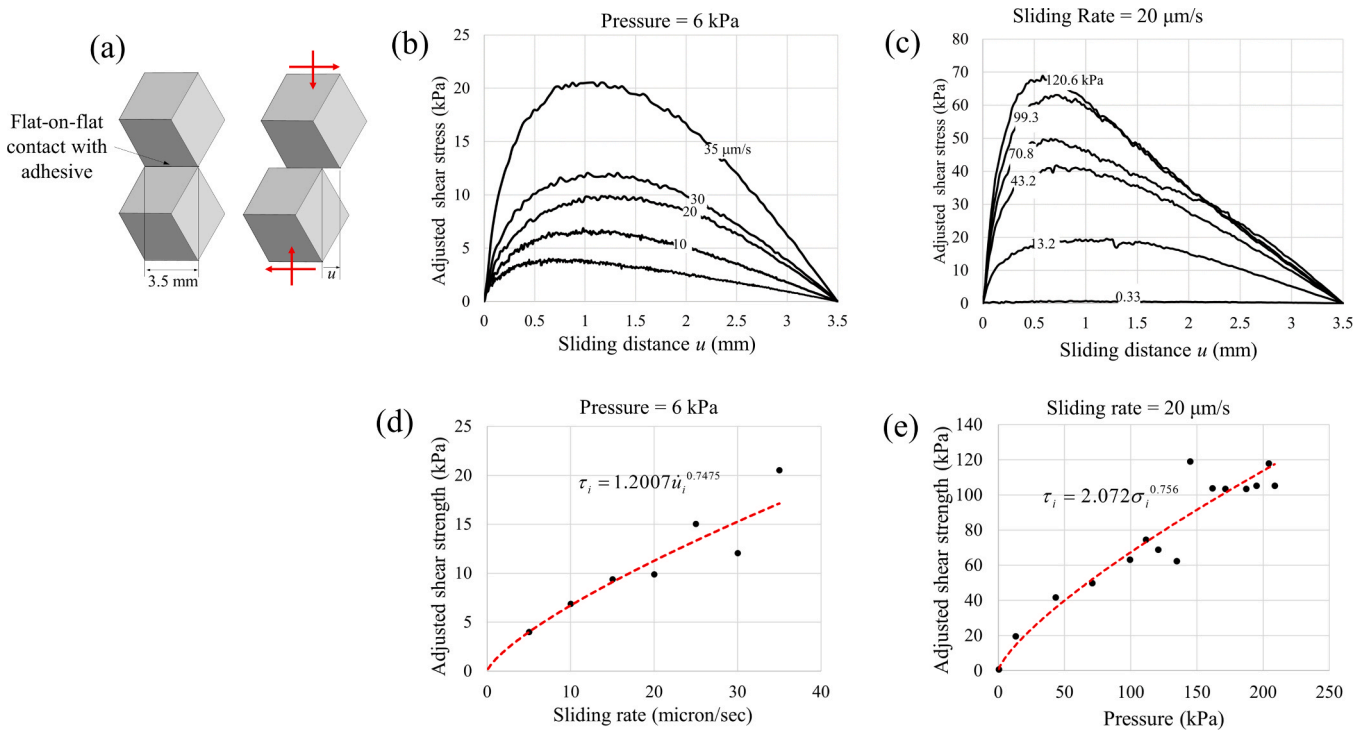

Fig. 4. Experiments and models for grain-on-grain interactions. (a) Diagram showing a pair of grains sliding on one another; (b-c) shear-sliding curves adjusted for the loss of contact area, and shear strength as function of (d) sliding rate and (e) normal pressure, with power law fits.

uniaxial stress σ_a is applied along an arbitrary direction with respect to the crystal. The resolved shear stress and resolved normal stress on each of the four available slip planes are calculated using stress transformation. The yield strength of the crystal also depends on the sliding speed of the individual grains, which we estimated from experiments using an image tracking algorithm. We measured a local sliding speed of 6 μm/sec for the 30 μm/sec compression speed, and 12 μm/sec for the 330 μm /sec compression speed. We then determined which of the available slip planes reaches the sliding criterion first, which we used to calculate the compressive yield strength of the crystal. We repeated the process by considering any loading direction in 3D for the crystal, which produced the 3D failure envelope shown on Fig. 5d. Fig. 5d show that the strength of the FCC crystal is strongly anisotropic. Along six directions the predicted yield strength is infinite. These directions correspond to the strongest "on-axis" direction, where buckling prevails in the experiments. Fig. 5e shows the 2D projection of the 3D failure envelope shown in Fig. 5d along the {111} plane for FCC. This 2D projections show that the model is in good agreement with experiments on "off-axis" samples at low and high rate (Fig. 5e). The nonlinear deformation of the cohesive granular crystal can therefore be captured with a "crystal plasticity" model, which highlights the strongly anisotropic strength of the crystal.

6. Summary

We have assembled, fabricated, and tested cohesive FCC granular crystals made of millimeter size rhombic dodecahedra grains. The pressure sensitive adhesive we used was strong enough to hold the grains together with no need for external confinement (container or vacuum bag), yet weak enough to prevent damage to the grains and ductile enough to enable large, controlled deformation with hardening and energy dissipation. These granular crystals are highly anisotropic. The on-axis cohesive FCC crystals were 20–60 times stronger than traditional randomly distributed spheres (RDS), and the off-axis cohesive FCC crystals were 4–5 times stronger than RDS. Where random spheres show a typical homogenous "flow" of grains under compressive loading, the cohesive granular crystals display a rich set of mechanisms: Nonlinear deformations, crystal plasticity reminiscent of atomistic mechanisms, cross-slip, shear-induced dilatancy, micro-buckling. We captured the anisotropic yield strength of the crystal using a cohesive granular plasticity model that accounts for the pressure and rate sensitivity of the adhesive, for the morphology of the available {111} slip planes in the FCC crystal, and for loading orientation. Interestingly, once tested the adhesive in these granular crystals could be dissolved and washed away, so that the individual grains could be recovered and recycled into new crystals with no loss of mechanical performance. The granular materials presented here are crystallized which makes them stronger than typical granular materials, but at the expense of adaptability and reconfigurability. They are therefore unsuitable for some robotic applications that rely on reconfigurability and large deformations, for example granular-based grippers [43,44]. The crystal plasticity mechanisms discussed here still confer the crystals with some malleability akin to ductile metals, which can be used for forming. The "model" granular materials presented here are based on polymeric grains and weak adhesives, but it is conceivable to fabricate grains made of much stronger materials (metals, ceramics) bonded by much stronger adhesives. For example, the granular crystal plasticity model we presented here predicts a yield strength exceeding 100 MPa for a granular crystal made of strong grains and epoxy at the interfaces, which compares with the strength of aluminum alloys, some composites, and concrete (in compression). These granular crystals could then find applications for rapid and versatile construction of static structures, or as modular light weight protective materials in a multitude of applications (e.g. buildings, body armor, vehicles, etc.). This approach to material design is also amenable to multiple options in terms of tunability and possible enhancements. For example, the overall performance of the crystals may be further enhanced by using more sophisticated adhesives akin to natural proteins in bone or nacre [45,46], or with fluids with interesting rheologies [47,48]. In addition, the fabrication and testing approach we present here for FCC cohesive granular crystals can also be extended to other crystalline forms (BCC, HCP, Diamond cubic), to crystals with defects (vacancies, grain boundaries), or also to granular

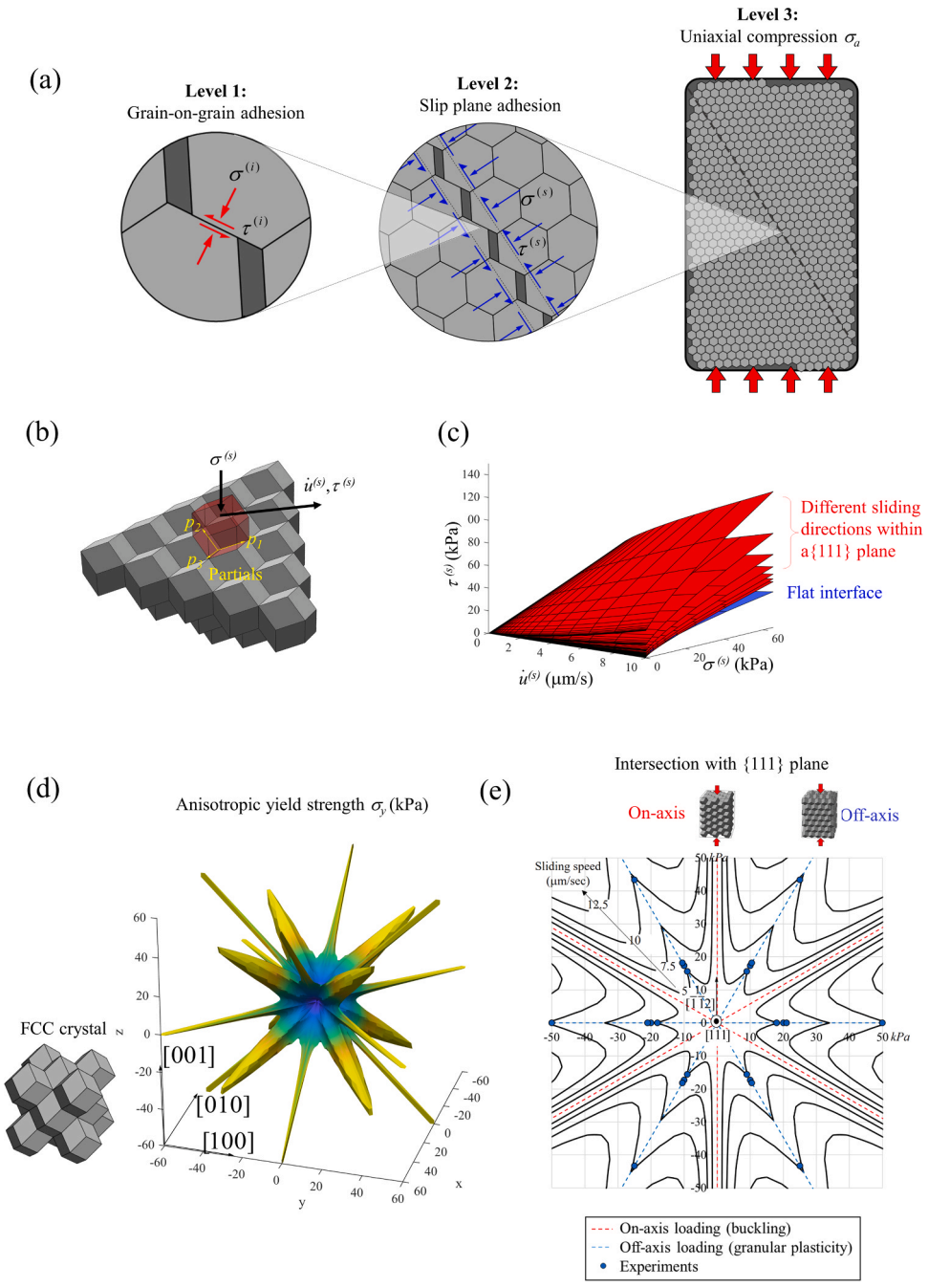

Fig. 5. A crystal cohesive plasticity model. (a) Micromechanics of deformation can be captured with a three-level approach that incorporates adhesion between individual grains, pressure and rate dependant shear response on slip planes, and resolved stresses and slip plane activation depending on loading orientation. (b) Sliding of an individual grain (in red) on a {111} plane in a FCC crystal; (c) shear strength on different slip planes as function of sliding rate and pressure. (d) Yield strength of FCC predicted by this model and displayed as 3D yield envelopes (the surface was colored to highlight the directions of higher strength, in yellow). (e) Section of these envelopes along the {111} plane (FCC) is also displayed. The model predicts forbidden directions for plasticity (where buckling occurs) and agrees well with experimental strengths in the off-axis directions.

and architected materials with more complex geometries, for example grains with non-planar faces [49–51], chiral crystals [52] or space filling "VoroNoodles" [53]. The individual grains, which are linear elastic in this study, could also be imparted with unusual properties such as auxetic behavior [54] or buckling instabilities [55] to even further enrich mechanical response and tunability.

CRediT authorship contribution statement

Ashta Navdeep Karuriya: Writing – review & editing, Writing – original draft, Visualization, Validation, Software, Methodology, Investigation, Formal analysis, Data curation. **Francois Barthelat:** Writing – review & editing, Writing – original draft, Visualization, Validation, Supervision, Software, Resources, Project administration, Methodology, Investigation, Funding acquisition, Formal analysis, Data curation, Conceptualization. **Jeremy Simoes:** Writing – original draft, Visualization, Validation, Methodology, Investigation.

Declaration of Competing Interest

The authors declare that they have no known competing financial interests or personal relationships that could have appeared to influence the work reported in this paper.

Data Availability

Data will be made available on request.

Acknowledgments

This work was sponsored by the University of Colorado Boulder, by the United States National Science Foundation (CMMI Award 2033991), and by the Army Research Office under Grant Number: W911NF-21–1–0175. The views and conclusions contained in this document are those of the authors and should not be interpreted as representing the official policies, either expressed or implied, of ARO or the U.S. Government. The U.S. Government is authorized to reproduce and distribute reprints for Government purposes notwithstanding any copyright notation herein.

References

[1] H.M. Jaeger, S.R. Nagel, R.P. Behringer, Granular solids, liquids, and gases, Rev. Mod. Phys. 68 (1996) 1259–1273, https://doi.org/10.1103/RevModPhys.68.1259.
[2] R.P. Behringer, B. Chakraborty, The physics of jamming for granular materials: a review, Rep. Prog. Phys. 82 (2018) 012601, https://doi.org/10.1088/1361-6633/aadc3c.
[3] F. Radjai, J.-N. Roux, A. Daouadji, Modeling granular materials: century-long research across scales, J. Eng. Mech. 143 (2017) 04017002, https://doi.org/10.1061/(ASCE)EM.1943-7889.0001196.
[4] R.P. Behringer, D. Bi, B. Chakraborty, A. Clark, J. Dijksman, J. Ren, J. Zhang, Statistical properties of granular materials near jamming, J. Stat. Mech. Theory Exp. 2014 (2014) P06004, https://doi.org/10.1088/1742-5468/2014/06/P06004.
[5] A.G. Athanassiadis, M.Z. Miskin, P. Kaplan, N. Rodenberg, S.H. Lee, J. Merritt, E. Brown, J. Amend, H. Lipson, H.M. Jaeger, Particle shape effects on the stress response of granular packings, Soft Matter 10 (2014) 48–59, https://doi.org/10.1039/C3SM52047A.
[6] P. Pierrat, H.S. Caram, Tensile strength of wet granula materials, Powder Technol. 91 (1997) 83–93, https://doi.org/10.1016/S0032-5910(96)03179-8.
[7] N. Mitarai, F. Nori, Wet granular materials, Adv. Phys. 55 (2006) 1–45, https://doi.org/10.1080/00018730600626065.
[8] M. Macaulay, P. Rognon, Viscosity of cohesive granular flows, Soft Matter 17 (2021) 165–173, https://doi.org/10.1039/D0SM01456G.
[9] S. Mandal, A. Gans, M. Nicolas, O. Pouliquen, Flows of cohesive granular media, EPJ Web Conf. 249 (2021) 01001, https://doi.org/10.1051/epjconf/202124901001.
[10] A. Gans, O. Pouliquen, M. Nicolas, Cohesion-controlled granular material, Phys. Rev. E 101 (2020) 032904, https://doi.org/10.1103/PhysRevE.101.032904.
[11] A. Gans, A. Abramian, P.-Y. Lagrée, M. Gong, A. Sauret, O. Pouliquen, M. Nicolas, Collapse of a cohesive granular column, J. Fluid Mech. 959 (2023) A41, https://doi.org/10.1017/jfm.2023.180.
[12] A. Hemmerle, M. Schröter, L. Goehring, A cohesive granular material with tunable elasticity, Sci. Rep. 6 (2016) 35650, https://doi.org/10.1038/srep35650.
[13] A. Hemmerle, Y. Yamaguchi, M. Makowski, O. Bäumchen, L. Goehring, Measuring and upscaling micromechanical interactions in a cohesive granular material, Soft Matter 17 (2021) 5806–5814, https://doi.org/10.1039/D1SM00458A.
[14] A. Schmeink, L. Goehring, A. Hemmerle, Fracture of a model cohesive granular material, Soft Matter 13 (2017) 1040–1047, https://doi.org/10.1039/C6SM02600A.
[15] F.X. Villarruel, B.E. Lauderdale, D.M. Mueth, H.M. Jaeger, Compaction of rods: relaxation and ordering in vibrated, anisotropic granular material, Phys. Rev. E 61 (2000) 6914–6921, https://doi.org/10.1103/PhysRevE.61.6914.
[16] L.K. Roth, H.M. Jaeger, Optimizing packing fraction in granular media composed of overlapping spheres, Soft Matter 12 (2016) 1107–1115, https://doi.org/10.1039/C5SM02335A.
[17] P.F. Damasceno, M. Engel, S.C. Glotzer, Predictive Self-Assembly of Polyhedra into Complex Structures, Science 337 (2012) 453–457, https://doi.org/10.1126/science.1220869.
[18] J. Henzie, M. Grünwald, A. Widmer-Cooper, P.L. Geissler, P. Yang, Self-assembly of uniform polyhedral silver nanocrystals into densest packings and exotic superlattices, Nat. Mater. 11 (2012) 131–137, https://doi.org/10.1038/nmat3178.
[19] E. Hascoët, H.J. Herrmann, V. Loreto, Shock propagation in a granular chain, Phys. Rev. E 59 (1999) 3202–3206, https://doi.org/10.1103/PhysRevE.59.3202.
[20] C. Daraio, V.F. Nesterenko, E.B. Herbold, S. Jin, Energy trapping and shock disintegration in a composite granular medium, Phys. Rev. Lett. 96 (2006) 058002, https://doi.org/10.1103/PhysRevLett.96.058002.
[21] C. Chong, M.A. Porter, P.G. Kevrekidis, C. Daraio, Nonlinear coherent structures in granular crystals, J. Phys. Condens. Matter 29 (2017) 413003, https://doi.org/10.1088/1361-648X/aa7672.
[22] M.A. Porter, P.G. Kevrekidis, C. Daraio, Granular crystals: nonlinear dynamics meets materials engineering, Phys. Today 68 (2015) 44–50, https://doi.org/10.1063/PT.3.2981.
[23] A. Parsa, C.S. O'Hern, R. Kramer-Bottiglio, J. Bongard, Gradient-based Design of Computational Granular Crystals, (2024). https://doi.org/10.48550/arXiv.2404.04825.
[24] H. Kocharyan, N. Karanjgaokar, Influence of lateral constraints on wave propagation in finite granular crystals, J. Appl. Mech. 87 (2020) 071011, https://doi.org/10.1115/1.4047004.
[25] K. Fu, Z. Zhao, L. Jin, Programmable granular metamaterials for reusable energy absorption, Adv. Funct. Mater. 29 (2019) 1901258, https://doi.org/10.1002/adfm.201901258.
[26] D. Yang, X. Chu, C. Xiu, Y. Pan, Influence of aspect ratio on wave propagation in granular crystals consisting of ellipse-shaped particles, Int. J. Appl. Mech. 15 (2023) 2250096, https://doi.org/10.1142/S175882512250096X.
[27] A.V. Dyskin, Y. Estrin, A.J. Kanel-Belov, E. Pasternak, Topological interlocking of platonic solids: a way to new materials and structures, Philos. Mag. Lett. 83 (2003) 197–203, https://doi.org/10.1080/0950083031000065226.
[28] T. Siegmund, Heterogeneous topologically interlocked materials: a new class of heterogeneous materials, Adv. Heterog. Mater. Mech. 2011 (2011) 0, in: ⟨https://www.dpi-proceedings.com/index.php/ichmm2011/article/view/22047⟩ (accessed July 12, 2023).
[29] M. Mirkhalaf, T. Zhou, F. Barthelat, Simultaneous improvements of strength and toughness in topologically interlocked ceramics, Proc. Natl. Acad. Sci. 115 (2018) 9128–9133, https://doi.org/10.1073/pnas.1807272115.
[30] M. Mirkhalaf, J. Tanguay, F. Barthelat, Carving 3D architectures within glass: exploring new strategies to transform the mechanics and performance of materials, Extrem. Mech. Lett. 7 (2016) 104–113, https://doi.org/10.1016/j.eml.2016.02.016.
[31] A.N. Karuriya, F. Barthelat, Granular crystals as strong and fully dense architectured materials, Proc. Natl. Acad. Sci. 120 (2023) e2215508120, https://doi.org/10.1073/pnas.2215508120.
[32] E-Rigid Form, ETEC (n.d.). ⟨https://envisiontec.com/material/e-rigid-form/⟩ (Accessed March 30, 2022).
[33] Aleene's Repositionable Tacky Spray 10 oz., Aleene's Prem. Glue (n.d.). ⟨https://www.aleenes.com/aleenes-repositionable-tacky-spray⟩ (Accessed July 21, 2023).
[34] S. Mapari, S. Mestry, S.T. Mhaske, Developments in pressure-sensitive adhesives: a review, Polym. Bull. 78 (2021) 4075–4108, https://doi.org/10.1007/s00289-020-03305-1.
[35] C. Creton, M. Ciccotti, Fracture and adhesion of soft materials: a review, Rep. Prog. Phys. 79 (2016) 046601, https://doi.org/10.1088/0034-4885/79/4/046601.
[36] C. Creton, Pressure-sensitive adhesives: an introductory course, MRS Bull. 28 (2003) 434–439, https://doi.org/10.1557/mrs2003.124.
[37] S. Sun, M. Li, A. Liu, A review on mechanical properties of pressure sensitive adhesives, Int. J. Adhes. Adhes. 41 (2013) 98–106, https://doi.org/10.1016/j.ijadhadh.2012.10.011.
[38] R. Verde, L. Grassia, A. D'Amore, Viscoelastic properties of soft adhesives, Macromol. Symp. 405 (2022) 2100270, https://doi.org/10.1002/masy.202100270.
[39] R. Villey, C. Creton, P.-P. Cortet, M.-J. Dalbe, T. Jet, B. Saintyves, S. Santucci, L. Vanel, D.J. Yarusso, M. Ciccotti, Rate-dependent elastic hysteresis during the peeling of pressure sensitive adhesives, Soft Matter 11 (2015) 3480–3491, https://doi.org/10.1039/C5SM00260E.
[40] A. Arrowood, M.A. Ansari, M. Ciccotti, R. Huang, K.M. Liechti, G.E. Sanoja, Understanding the role of crosslink density and linear viscoelasticity on the shear failure of pressure-sensitive-adhesives, Soft Matter 19 (2023) 6088–6096, https://doi.org/10.1039/D3SM00562C.
[41] F. Sosson, A. Chateauminois, C. Creton, Investigation of shear failure mechanisms of pressure-sensitive adhesives, J. Polym. Sci. Part B Polym. Phys. 43 (2005) 3316–3330, https://doi.org/10.1002/polb.20619.
[42] V. Pandey, A. Fleury, R. Villey, C. Creton, M. Ciccotti, Linking peel and tack performances of pressure sensitive adhesives, Soft Matter 16 (2020) 3267–3275, https://doi.org/10.1039/C9SM02172H.
[43] E. Brown, N. Rodenberg, J. Amend, A. Mozeika, E. Steltz, M.R. Zakin, H. Lipson, H. M. Jaeger, Universal robotic gripper based on the jamming of granular material, Proc. Natl. Acad. Sci. 107 (2010) 18809–18814, https://doi.org/10.1073/pnas.1003250107.
[44] Y. Wang, L. Li, D. Hofmann, J.E. Andrade, C. Daraio, Structured fabrics with tunable mechanical properties, Nature 596 (2021) 238–243, https://doi.org/10.1038/s41586-021-03698-7.
[45] F. Barthelat, Z. Yin, M.J. Buehler, Structure and mechanics of interfaces in biological materials, Nat. Rev. Mater. 1 (2016) 1–16, https://doi.org/10.1038/natrevmats.2016.7.
[46] Z. Yin, F. Hannard, F. Barthelat, Impact-resistant nacre-like transparent materials, Science 364 (2019) 1260–1263, https://doi.org/10.1126/science.aaw8988.
[47] R.W. Style, R. Tutika, J.Y. Kim, M.D. Bartlett, Solid–liquid composites for soft multifunctional materials, Adv. Funct. Mater. 31 (2021) 2005804, https://doi.org/10.1002/adfm.202005804.
[48] Y.S. Lee, E.D. Wetzel, N.J. Wagner, The ballistic impact characteristics of Kevlar® woven fabrics impregnated with a colloidal shear thickening fluid, J. Mater. Sci. 38 (2003) 2825–2833, https://doi.org/10.1023/A:1024424200221.

[49] Y. Estrin, V.R. Krishnamurthy, E. Akleman, Design of architectured materials based on topological and geometrical interlocking, J. Mater. Res. Technol. 15 (2021) 1165–1178, https://doi.org/10.1016/j.jmrt.2021.08.064.
[50] A.S. Dalaq, F. Barthelat, Manipulating the geometry of architectured beams for maximum toughness and strength, Mater. Des. 194 (2020) 108889, https://doi.org/10.1016/j.matdes.2020.108889.
[51] I. Koureas, M. Pundir, S. Feldfogel, D.S. Kammer, The key to the enhanced performance of slab-like topologically interlocked structures with non-planar blocks, Int. J. Solids Struct. 285 (2023) 112523, https://doi.org/10.1016/j.ijsolstr.2023.112523.
[52] D.Y. Kim, T. Siegmund, Chirality in topologically interlocked material systems, Mech. Mater. 191 (2024) 104956, https://doi.org/10.1016/j.mechmat.2024.104956.
[53] M. Ebert, E. Akleman, V. Krishnamurthy, R. Kulagin, Y. Estrin, VoroNoodles: topological Interlocking with Helical Layered 2-Honeycombs, Adv. Eng. Mater. 26 (2024) 2300831, https://doi.org/10.1002/adem.202300831.
[54] D. Haver, D. Acuña, S. Janbaz, E. Lerner, G. Düring, C. Coulais, Elasticity and rheology of auxetic granular metamaterials, Proc. Natl. Acad. Sci. 121 (2024) e2317915121, https://doi.org/10.1073/pnas.2317915121.
[55] A. Djellouli, B.V. Raemdonck, Y. Wang, Y. Yang, A. Caillaud, D. Weitz, S. Rubinstein, B. Gorissen, K. Bertoldi, Shell buckling for programmable metafluids, Nature (2024).